Study of the rheological properties of the retropulsive jet build by the antral contraction wave in a simplified artificial stomach

Damien Dufour[1], Franz X. Tanner[2], Kathleen Feigl[2], Yasushi Takeda[1], Stéphane Fischer[3], and Erich J. Windhab[1]

[1] Laboratory for Food Process Engineering (FPE), Swiss Federal Institute of Technology Zurich, Zurich 8092, Switzerland
[2] Department of Mathematical Sciences, Michigan Technological University, Houghton, MI 49931-1295, U.S.A.
[3] Ubertone SA, 67000 Strasbourg, France

The digestion of food is a process composed of different phases. A better knowledge of the entire process allows to design tailor made foods. This study is focused on the retropulsive jet generated by the contractions of the stomach and the impact of this flow field to the disintegration of the food. The antral contraction wave is moving at a constant speed toward the pylorus and shrinks at the same time. A prototype of a stomach was built to mimic the displacement of these contractions, in a simpler way. The flow field in the prototype was measured by UVP and compared with numerical simulations. Then, the simulations were used to compute the local stress applied on the fluid. Experiments with Newtonian fluids and two contractions with relative occlusions (RO) of 0.6 and 0.75 shown good agreement with the simulations. The elongation rate was higher with a RO of 0.75. A higher translation speed of the contraction (RO=0.6) allowed to increase the elongation rate.

Keywords: Artificial stomach, Retropulsive jet, UVP, ACW, Non-Newtonian fluid

1. Introduction

The digestion of food in the gastro-intestinal tract is a long process, going through many steps [1]. The mouth and the stomach are the major actors in the disintegration of food. Then, the different sections of the intestine ensure the final break down and the absorption of the nutriments. The disintegration of food in the stomach is a combination of two different actions [2]. First, the chemical action (e.g. saliva, gastric juices and enzymes) helps to soften the ingested food. The second action is mechanical, the stomach produces antral contraction waves (ACW) [1,3], which have different functions. One role is the transportation. From the storage part of the stomach, called the corpus, a small part of the bolus (ingested food) moves toward the antrum. In the antrum, the ACW shrinks and produces a retropulsive jet. This jet helps the chemical reaction by mixing the content of the stomach. Finally, at the end of the antrum, a small part of the chyme is transferred to the intestine, through the pylorus, to start the next digestive step. On top, the retropulsive jet induces high elongation and shear stresses in the fluid. This stress is transferred to the solid particles and break when the threshold value of the particle is reached.

The chemical action in the stomach is well known. Few prototypes of artificial stomachs were created [6-7]. These reproduce the chemical conditions happening in the stomach. Some of them simulate a mechanical action but it is often over simplified [8]. In the last few decades, the field of computational fluid dynamics made a lot of improvements and it is now able to compute complex systems like a human stomach. Several models were developed, in 2D and 3D, which shown the action of the ACW on the flow field [4,5]. These studies proved the

impact of the rheological properties of the fluid on the shape of the jet, i.e. the stress applied to the particles. However, due to the lack of accurate *in vivo* measurement of the retropulsive jet, direct comparisons with simulations are impossible. Only ultrasonography or MNR imaging are allowed on humans [9-11], which do not provide a sufficient resolution of the flow field.

A device imitating the dynamic flow of the stomach, will have two benefits. It will help to build a more elaborate artificial stomach, which is able to reproduce the chemical environment and the flow field of the stomach. In addition, such device can reproduce flows of the stomach and can be used to validate results from simulations. This study aims to better understand the retropulsive jet created by the displacement of the ACW. To this end, a prototype of an artificial stomach was made. The dimensions are close to a real stomach, and large enough to allow the insertion of the UVP sensors. The prototype was tested with Newtonian and non-Newtonian fluids. The velocity along the center line in the antrum part was measured by UVP and compared with simulations.

2. Material and method

2.1 Prototype of stomach

The artificial stomach developed for this study was made of Plexiglas, as shown on Fig. 1b. It was built by the workshop of the FPE laboratory. The main part is a cuboid, which stands for the corpus of the stomach. The cuboid has a squared base of 120*120mm² and 150mm height. This is connected to a cylinder of diameter D and length L, representing the antrum. The cylinder was pierced in a 60mm squared rod. On Fig. 1a are represented two hollow pistons, which are used to reproduce the ACW. The pistons were 3D printed

(Sculpteo, Paris, France). The dimensions are detailed in Table 1. The cross section is a parabolic shape. Two distinct inner diameters, D_i, allow to reproduce different states of contraction of the ACW [7]. The relative occlusion (RO) is calculated according to Eq. (1). One piston is placed in the cylinder and driven with two stainless steel rods, going through the back wall of the tank. These rods are moved by a stepper motor and a screw-nut system. The outer diameter of each piston is 0.2mm smaller than D, to avoid friction with the cylinder. The pylorus (left side on Fig. 1b) is drilled to insert the UVP sensors (Tr1), aligned with the central-axis of the cylinder. In addition, a target (8mm diameter PVC cylinder) was placed in the tank, to measure the sound speed in the fluid.
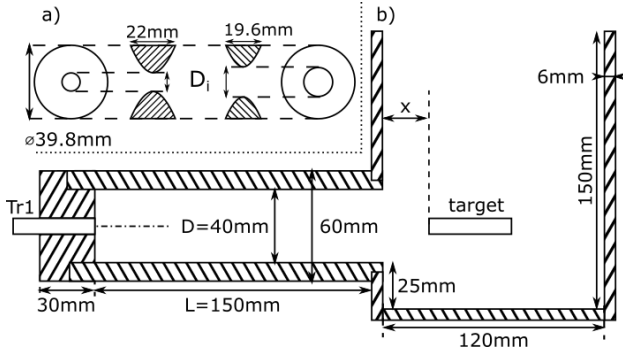

Figure 1: (a) Schematic of the axisymmetric contractions used in the artificial stomach. The inner diameters D_i are specified in Table 1. (b) Schematic of the artificial stomach used for the experiments. The system used to translate the contractions is located on the right-hand side of the prototype (not shown here).

The average human stomach is about 0.94L, ranging from 0.25L to 1.7L [7]. The nominal volume of the prototype is 1.5L, which corresponds to 90mm of fluid in the tank. The ACW are formed roughly 150mm away from the pylorus [7,8]. The length of the artificial antrum is also 150mm, which is long enough to reach the steady flow of the jet. The inner diameters of the contractions were limited by the diameter of the ultrasound beam, to reduce interception with the piston ($D_i \geq 10$mm). Due to the maximal RO we studied (0.75), the diameter D of the cylinder was constrained to 40mm.

$$RO = 1 - \frac{D_i}{D} \qquad (1)$$

Table 1: Dimensions of the hollow pistons used as ACW.

D_i (mm)	Outer dia. (mm)	Width (mm)	RO
10	39.8	22	0.75
16	39.8	19.6	0.6

2.2 Simulations

A numerical 2D model of the cylinder was done, with a mesh size of 213 x 32 x 1cells. The mesh describes half of the cylinder. The result of the simulation is equivalent to a 3D cylinder due to an axisymmetric computation.

The ACW was modelised as a progressive wave, by deforming the wall. The velocity on the walls is null everywhere except at the surface of the contraction. In this case, the boundary velocity equals to the translation speed of the contraction. The simulations were made by F. Tanner and K. Feigl from the Michigan Technological University.

2.3 UVP measurement

The UVP device is a UB-lab from the Ubertone company (Strasbourg, France). The transducers are from Imasonic (Besancon, France). Two types of transducers were used, which are described in Table 2.

Table 2: Characteristics of the ultrasound sensors used for the experiments. The half opening angle is given at -6dB of beam amplitude and goes up to 5.2° when the amplitude is null.

Central frequency (MHz)	Active element dia. (mm)	Outer dia. (mm)	Half opening angle (°)	Near field (mm)
4	5	8	2.2	17
8	2.5	8	2.2	8.5

2.4 Newtonian fluid

The Newtonian fluid used was a glycerin solution, with a 27% volume concentration. Glycerin was added to tune the buoyancy of the particles used as acoustic reflectors. These particles were from Metflow (Lausanne, Switzerland). The density was 1.07kg/L and the diameter range from 80µm to 200µm. A small amount of these particles were added to the solution (<0.5%). The viscosity of the final solution (27% glycerin + particles) was 3.2mPa.s and the sound speed was 1645m/s.

2.5 Shear thinning fluid

Two non-Newtonian solutions were prepared with guar gum, at 0.5% and 1% mass concentration. No acoustic reflectors were added and the sound speed was around 1485m/s. The shear viscosity of the solution was measured with a MRC-300 rheometer (Anton Paar, Ostfildern, Germany). The viscosity was measured over 5 decades of shear rate, from 10^{-2} to $10^3 s^{-1}$, and after a pre-shear at $100 s^{-1}$ for 10s. A Bird-Carreau model, defined by Eq. (2), was fitted on the viscosity data. The results in Table 3 were used to compute the simulation.

$$\eta(\dot{\gamma}) = \eta_\infty + (\eta_0 - \eta_\infty)\left(1 + (\lambda\dot{\gamma})^2\right)^{\frac{(n-1)}{2}} \qquad (2)$$

η_∞ is the infinite shear viscosity and η_0 is the null shear viscosity. λ is the relaxation time and n is the power-law index. As the solution was water based, the infinite viscosity was set to 1mPa.s.

Table 3: Results of the Bird-Carreau fit from guar solutions.

Guar con. (%)	η_0 (Pa.s)	λ (s)	n	R^2
0.5	0.247	0.188	0.523	0.993
1	6.18	1.10	0.355	0.954

2.6 Experimental

Tr1 was inserted at the pylorus. While the stomach was filled, large air bubbles were flushed from the cylinder. The stomach was placed on the bench and the contraction was connected to the screw-nut system to control the displacement. The target was inserted in the tank and the x distance, on Fig 1b, was measured. The sound speed was calculated, with an error below 1%. The contraction was set to the initial position and halted 10 seconds to stabilize the flow in the stomach. The contraction started moving with the defined speed. The velocity of the fluid was recorded by UVP over time, using one setup from Table 4. The Doppler spectrum was computed from the I and Q Doppler data. The center line velocity was extracted from the Doppler spectrum using a threshold on the intensity of the spectrum [12]. Due to a broad range of velocities in the retropulsive jet, the threshold T was kept low (e.g. 2dB) to only select the higher velocities (i.e. center line velocity). The velocity was calculated, for each position (cell), according to the Eqs. (3) and (4).

$$v_{fft} = \frac{c}{2f_0} \frac{\sum f_i S(f_i)}{\sum S(f_i)} \qquad (3)$$

$$S(f_i) = \begin{cases} S(f_i), & for \quad 10\log_{10}\left(\frac{S_{max}}{S(f_i)}\right) \le T \\ 0, & otherwise \end{cases} \qquad (4)$$

Where c is the speed of sound in the fluid, f_0 is the emission frequency. f_i and $S(f_i)$ are respectively the frequency i of the Doppler spectrum and the spectral density associated to this frequency. S_{max} is the maximum of the spectral density, for a given cell. An offset of 1e-20 is added to $S(f_i)$ to avoid divisions by zero.

Table 4: Two configurations of the UVP device used for the experiments. The amplification was fixed at 60dB over all cells. The 4.17MHz setup was used with the 4MHz transducer and the 7.5MHz setup, with the 8MHz transducer. The distances are given for a sound speed of 1480m/s.

f_0 MHz	PRF kHz	Samples	Pulse mm	1st cell mm	Δ cell mm	N cells
4.17	0.73	128	0.79	80.2	0.355	100
7.5	1.1	128	0.79	40.2	0.355	90

The 2D velocity vector measurement is not shown here because of challenges induced by the contraction. An echo on the piston creates a strong shift on the Doppler spectrum which completely biased the 2D reconstruction. Similar effect appends on the 10mm case, on Fig. 2. A filtering of the Doppler data is needed to erase this echo.

3. Results and Discussion

3.1 Glycerin solution

The first experiments were done with the 4MHz transducer. The 10mm contraction was running at 2.5mm/s, the 16mm contraction was tested at 2.5mm/s and 7.5mm/s. The Reynolds numbers were, respectively,

167, 107 and 268. Fig. 2 shows the measured data and the simulations. The UVP data are a collection of the measured data over time. The observable window is about 40mm long, thus it cannot cover the entire jet instantaneously. To overcome this, the observable window was positioned far from the pylorus. While the contraction was moving toward the pylorus, the tail of the jet was recorded. The disadvantage of this method is that the beam covers a wide area. With the 10mm contraction (black squares), the ultrasound beam intercepts the hollow piston and the measurement is disturbed (around 46mm on Fig. 2). With the 16mm contraction, the intersection with the beam is smaller, so the profile of the jet is less disturbed. In every case, the tail of the jet (from 60 to 120mm) is also disturbed. This is due to the different velocities which compose the jet and creates a non-symmetric velocity distribution in the Doppler spectrum. The post processing of the Doppler spectrum removed most of the echo from the 16mm contraction, however, the disturbance was too high on the 10mm contraction. Regarding the tail of the jet, computing the velocity with Eqs. (3) and (4), plus a low threshold, allowed to reduce the effect of the non-symmetric velocity distribution in the tail, but increased the noise on the final result.
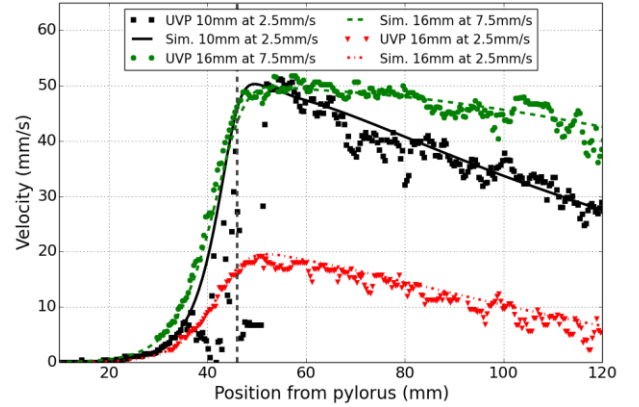

Figure 2: Measurement and simulation of the 27% glycerin solution with different RO and displacement speed of the contraction. The center of the contraction is located at 46mm, shown by the vertical gray dashed line. Positive velocity means that the fluid is going away from the pylorus.

The elongation rate, on the center line, was computed from the simulations and displayed on Fig. 3. The 10mm contraction shown the highest elongation rate, which is expected as the fluid stretches more to go through the smallest opening. In addition, the 16mm contraction shows that the elongation rate can be tuned by adjusting the speed of the contraction. The aim of increasing the speed of the contraction is to be able to reproduce the shrinkage of the ACW. As this prototype works with fixed opening contractions, adjusting the speed allows to change the stress applied on the fluid during the experiment. To compute the stress applied on the particles, the shear rate needs to be measured from the simulation. The total stress in the fluid can be calculated by combination of the shear stress and elongation stress.
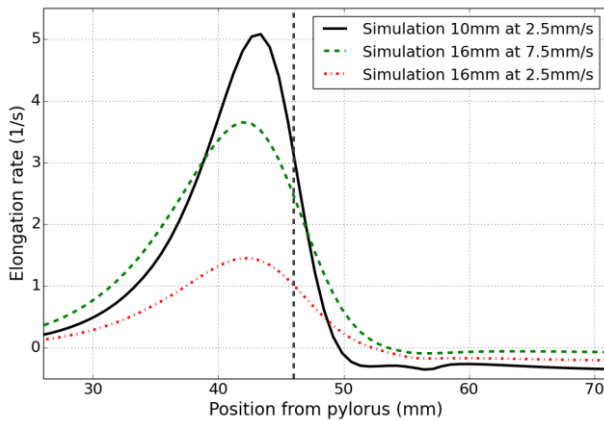
Figure 3: Elongation rate in the retropulsive jet, computed with the data from the simulations. The center of the contraction is symbolized by the vertical gray dashed line, at 46mm.

3.2 Guar solutions

The 0.5% and 1% guar solutions were tested with the 16mm contraction at 2.5mm/s and 7.5mm/s. The results are shown on Fig. 4. The length of the jet was much shorter compared to the Newtonian case. This was expected because of the higher viscosity, thus the damping increased. In addition, the higher viscosity increased the pressure between the contraction and the pylorus [7]. As a consequence, the fluid reached a higher velocity. In these cases, the maximum speed was about 30% higher compared to the jet from the 27% glycerin. The interesting fact is that increasing the guar concentration (e.g. zero-shear viscosity) had an unexpected effect on the top speed of the jet. As said before, a higher viscosity increases the speed of the jet. But, the maximum velocity of the 1% guar solution is slightly under the 0.5% solution. Further work and simulations must be done to better understand this phenomenon with the Non-Newtonian fluids.
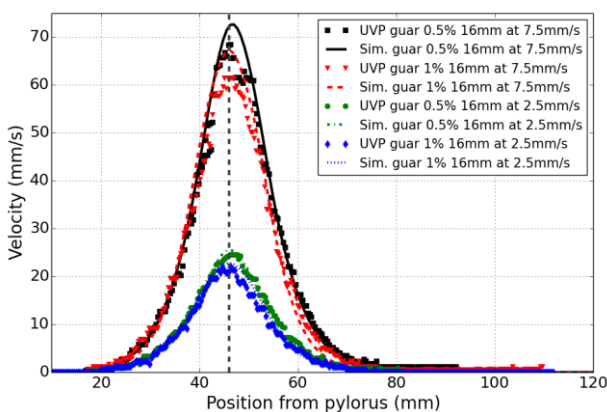

Figure 4: Retropulsive jet produced with a guar solution, measurements and simulations. Different concentrations and several displacement speeds with the 16mm contraction are shown. The middle of the contraction is situated at 46mm, represented by the vertical gray dashed line.

The trial with the 0.5% guar at 2.5mm/s was recorded at 7.5MHz, close to the pylorus. The other trials were recorded at 4MHz. The Doppler spectrogram at 7.5MHz

shown a velocity distribution which was less dispersed, than the 4MHz measurement. The narrow beam of the 8MHz transducer measures the velocities in the fluid closer from the center line. Thus the range of velocities seen by the beam is reduced compared to the 4MHz transducer. But the optimal result is obtained when the measurement window is close from the pylorus, thus the observable length is limited, about 80mm from the pylorus. As a consequence, the 8MHz measurement is better with viscous fluid, when the jet is short.

5. Conclusion

A prototype of a stomach was build, with dimensions close to the human stomach. The measurements done with the Newtonian fluid present a good match with the simulations. This validate the numerical model used for the simulation. With a RO of 0.75 and a Newtonian fluid (3.2mPa.), the jet reached a maximum velocity of 50mm/s and an elongation rate of $5s^{-1}$. With the 16mm contraction, the elongation rate was tuned by the adjusting the speed of the contraction. The advantage of such property is to simulate the shrink motion of the ACW with an accelerated solid contraction. The shear forces will be analyzed and added to the elongation stress. The stress induced by the fluid will be calculated and tested experimentally by droplet breakup experiment.

References

[1] Kong. F *et al.*: Disintegration of Solid Foods in Human Stomach, Journal of Food Science Vol. 73(5), R67-80 (2008).
[2] Camilleri M: Integrated Upper Gastrointestinal Response to Food Intake, Gastroenterology Vol. 131 (2), 640-658 (2006).
[3] Keinke O *et al.*: Mechanical Factors Regulating Gastric Emptying of Viscous Nutrient Meals in Dogs, Quarterly Journal of Experimental Physiology Vol. 69, 781-795 (1984).
[4] Kong F *et al.*: A Model Stomach System to Investigate Disintegration Kinetics of Solid Foods during Gastric Digestion, Journal of Food Science, Vol. 73 (5), E202-210 (2008).
[5] Kong F *et al.*: A Human Gastric Simulator (HGS) to Study Food Digestion in Human Stomach, Journal of Food Science, Vol. 75 (9), E627-635 (2010).
[6] Yoo JY *et al.*: GIT Physiochemical Modeling – A Critical Review, International Journal of Food Engineering Vol. 2(4), art. 4 (2006).
[7] Ferrua MJ *et al.*: Modeling the Fluid Dynamics in a Human Stomach to Gain Insight of Food Digestion, Journal of Food Science Vol.75 (7), R151-162 (2010).
[8] Pal A *et al.*: Gastric flow and mixing studied using computer simulation, Proc. R. Soc. Lond. B 271, 2587-2594 (2004).
[9] Schulze K: Imaging and modelling of digestion in the stomach and the duodenum, Neurogastroenterology & Motility 18, 172-183 (2006).
[10] Steingoetter A *et al.*: Imaging gastric structuring of lipid emulsions and its effect on gastrointestinal function: a randomized trial in healthy subjects, American Journal of Clinical Nutrition (2015).
[11] Berstad A *et al.*: Ultrasonography of the Human Stomach, Scandinavian Journal of Gastroenterology, 31:sup220, 75-82 (1996).
[12] Sirmans D *et al.*: Numerical Comparison of Five Mean Frequency Estimators, Journal of Applied Metrology, Vol. 14, 991-1003 (1975).